Available online at www.sciencedirect.com
SCIENCE DIRECT
International Journal of Mass Spectrometry 249–250 (2006) 462–472
International Journal of Mass Spectrometry
www.elsevier.com/locate/ijms

Mechanisms of peptide fragmentation from time- and energy-resolved surface-induced dissociation studies: Dissociation of angiotensin analogs

Julia Laskin [a,*], Thomas H. Bailey [b,1], Jean H. Futrell [c]

[a] *Pacific Northwest National Laboratory, Fundamental Science Directorate, P.O. Box 999 (K8-88), Richland, WA 99352, USA*
[b] *Department of Chemistry and Biochemistry, University of Delaware, Newark, DE 19716, USA*
[c] *Pacific Northwest National Laboratory, Office of Chief Research Officer, P.O. Box 999, Richland, WA 99352, USA*

Received 22 September 2005; received in revised form 3 November 2005; accepted 8 November 2005
Available online 20 December 2005

Dedicated to the memory of Prof. Chava Lifshitz – our colleague, mentor, and a dear friend.

Abstract

Energetics and mechanism of dissociation of singly protonated angiotensin III (RVYIHPF) and its analogs RVYIFPF, RVYIYPF, RVYIHAF and RVYIHDF was studied using surface-induced dissociation (SID) in a Fourier transform ion cyclotron resonance mass spectrometer (FT-ICR MS) specially configured for studying ion activation by collisions with surfaces. The energetics and dynamics of peptide fragmentation were deduced by modeling the time- and energy-resolved survival curves for each precursor ion using an RRKM-based approach developed in our laboratory. Fragmentation mechanisms were inferred from comparison of time- and energy-resolved fragmentation efficiency curves (TFECs) of different fragment ions followed by RRKM modeling of dissociation of angiotensin III into six major families of fragment ions. Detailed modeling demonstrated that dissociation of these peptides is dominated by loss of ammonia from the precursor ion and characterized by a high-energy barrier of 1.6 eV. Loss of NH_3 and subsequent rearrangement of the MH^+-NH_3 ion results in proton mobilization and release of ca. 30 kcal/mol into internal excitation of the MH^+-NH_3 ion. The resulting highly excited ion accesses a variety of non-specific dissociation pathways with very high rate constants. Fast fragmentation of excited MH^+-NH_3 ion forms a variety of abundant b_n-NH_3 and a_n-NH_3 fragment ions. Abundant XH and HX internal fragments are also formed, reflecting the stability of histidine-containing diketopiperazine structures.

Keywords: Surface-induced dissociation; Protonated peptide; Fragmentation mechanism; Fragmentation energetics; FT-ICR MS

1. Introduction

Dissociation of peptide ions in the gas phase is an active area of research in mass spectrometry. Mechanistic understanding of fragmentation of singly and multiply protonated peptides provides an important background for peptide sequencing and protein identification using tandem mass spectrometry (MS/MS) [1]. Structural information is extracted from the identification of sequence-specific fragments that originate from bond cleavages along peptide backbone. Gas-phase fragmentation of protonated peptides is typically dominated by cleavages of peptide (amide) bonds resulting in formation of b and y ions if the charge remains on the N-terminus or C-terminus, respectively. Loss of small molecules such as CO, NH_3 and H_2O from the protonated peptide and from its subsequent shorter chain fragments is commonly observed in tandem mass spectra. Internal fragments and immonium ions resulting from simultaneous or consecutive rupture of two peptide bonds are also commonly observed in MS/MS spectra. Current understanding of gas-phase ion chemistry leading to the observed fragmentation of peptide ions in mass spectrometry has been summarized in a number of commentary articles [2–5] and a recent review [6].

Experimental fragmentation patterns are influenced to varying degrees by a number of factors, including the method of ion activation and the resulting internal energy distribution of the excited ions, the intrinsic parameters of the ion such as the number of vibrational degrees of freedom (DOF) and the energetics and dynamics of each individual dissociation pathway, the timescale characteristic of the mass analyzer and possible mass discrimination. Detailed understanding of such a multidimensional problem is extremely challenging. Two additional complications

* Corresponding author. Tel.: +1 509 376 4443; fax: +1 509 376 3650.
E-mail address: Julia.Laskin@pnl.gov (J. Laskin).
[1] Present address: Metara Inc., 1225 E. Arques Ave., Sunnyvale, CA 94085, USA.

1387-3806/$ – see front matter © 2005 Elsevier B.V. All rights reserved.
doi:10.1016/j.ijms.2005.11.007

for understanding the dissociation behavior of large ions are the characteristically large kinetic shift (KS) [7] – the internal energy in excess of the dissociation energy required to produce detectable dissociation of a polyatomic ion on the time-scale of the mass spectrometer – and the relatively slow, stepwise ion activation methods employed in most MS/MS experiments [8]. We have previously demonstrated that fragmentation via the lowest-energy reaction channel efficiently competes with slow activation when competing reactions have substantially higher dissociation energies. This results in effective discrimination against high-energy channels and much lower ion yields or complete deletion of these channels in the MS/MS spectrum [9].

We have also argued that surface-induced dissociation (SID) offers significant advantages over slow activation methods for investigating mechanisms of peptide ion dissociation. In particular, SID resulting from collisions of ions with semiconductive surfaces of self-assembled monolayers (SAMs) [10,11] provides an efficient means for very fast, single-step excitation of the ion in which internal energy deposition occurs in a few picoseconds or less [12]. Coupling SID with a Fourier transform ion cyclotron resonance mass spectrometer (FT-ICR MS) provides the additional distinct advantage of long and variable reaction time (milliseconds to seconds), both greatly reducing the KS and enabling access to the lowest-energy dissociation pathways for large molecules [13,14]. Collision energy-resolved SID studies provide important information on the appearance energies of fragment ions and competition between different dissociation pathways. The ability to perform kinetic studies on the FT-ICR instrument adds a level of dimensionality to the SID experiment that cannot be achieved in an instrument with a fixed reaction time. It has been observed that several fragments can have similar appearance energies, yet exhibit very different kinetic behavior. Clearly time- and energy-resolved SID experiments provide very detailed information on the fragmentation of large ions.

In this work we present a detailed analysis of time- and energy-resolved fragmentation of singly protonated angiotensin III and its analogs. Experimental results are analyzed quantitatively using RRKM-based modeling described elsewhere [15,16]. This approach has been previously used for extracting total decomposition rates for a variety of model peptides [17–19]. Here we extend it to examine relative rates of different dissociation pathways. While it is impossible to model each separate reaction channel, we shall analyze the trends and propose mechanisms of formation for distinct families of fragment ions.

2. Experimental

SID experiments were conducted on a specially fabricated 6T FT-ICR mass spectrometer described elsewhere [20]. The instrument is equipped with a high-transmission electrospray source, consisting of an ion funnel interface [21] followed by three quadrupoles that provide for pressure drop and ion bunching, mass selection and ion storage, respectively. The SID target is introduced through a vacuum interlock assembly and is positioned at the rear trapping plate of the ICR cell. Both the instrument and SID experimental protocol have been detailed elsewhere [20] and will be only briefly outlined below.

Ions are electrosprayed, at atmospheric pressure, into the end of a heated stainless steel capillary tube. The ion funnel that follows the capillary provides highly efficient ion transfer into the high vacuum region of the mass spectrometer. Three quadrupoles following the ion funnel provide collisional focusing, mass selection of the ion of interest and accumulation of ions external to the ICR cell. Typical accumulation times are in the range of 0.3–0.8 s. The third (accumulation) quadrupole is held at elevated pressure (about 2×10^{-3} Torr) for collisional relaxation of any internal energy possessed by ions generated by electrospray ionization prior to their injection into the ICR cell.

After accumulation, the ions are extracted from the third quadrupole and transferred into the ICR cell where they collide with the surface. Scattered ions are captured by raising the potentials on the front and rear trapping plates of the ICR cell by 10–20 V. Time-resolved mass spectra were acquired by varying the delay between the gated trapping and the excitation/detection event (the reaction delay). The reaction delay was varied from 1 ms to 1 s. Immediately following the fragmentation delay, ions were excited by a broadband chirp and detected. The collision energy is defined by the difference in the potential applied to the accumulation quadrupole and the potential applied to the rear trapping plate and the SID target. The ICR cell can be offset above or below ground by as much as ±150 V. Lowering the ICR cell below ground while keeping the potential on the third quadrupole fixed increases collision energy for positive ions.

Experimental control is accomplished with a MIDAS data station [22]. MIDAS is used to control the voltages and timing of the source and transfer optics, as well as ion manipulation in the ICR cell. An automated script was written to allow for unattended acquisition of kinetic data. The script was used to vary the fragmentation delay and collision energy of the experiment. Reactions delays of 1 ms, 5 ms, 10 ms, 50 ms, 0.1 s and 1 s were studied. Typical experiments involved changing the collision energy across a relatively wide range from 15 eV to 65 eV. The automated script allowed for acquisition of SID spectra across the entire range of collision energies, in 1 eV increments, at each of the six fragmentation delays. Time-dependent survival curves were constructed from experimental mass spectra by plotting the relative abundance of the precursor ion as a function of collision energy for each delay time.

The self-assembled monolayer (SAM) surface was prepared on a single gold{1 1 1} crystal (Monocrystals, Richmond Heights, OH) using a standard procedure. The target was cleaned in a UV cleaner (Model 135500, Boekel Industries Inc., Feasterville, PA) for 10 min and allowed to stand in a 1 mM ethanol solution of FC_{12}, ($CF_3(CF_2)_9C_2H_4SH$), for 24–36 h. The target was removed from the SAM solution and ultrasonically washed in ethanol for 10 min to remove extra layers.

Angiotensin III (RVYIHPF) was purchased from Sigma. Angiotensin III analogs (RVYIHAF, RVYIHDF, RVYIFPF and RVYIYPF) were purchased from Peptron Inc. (Taejon, South Korea). All samples were dissolved in a 70:30 (v/v) methanol:water solution with 1% acetic acid. A syringe pump (Cole Parmer, Vernon Hills, IL) was used for direct infusion of

the electrospray samples at flow rates ranging from 20 μL/h to 50 μL/h.

2.1. RRKM modeling

The survival curves (SCs) representing the relative abundance of the parent ion as a function of collision energy were modeled using an RRKM-based approach developed by our group [15,16]. We modeled separately time-dependent (slow) and time-independent (fast) kinetics and used two dissociation rate constants for the total ion decomposition, as indicated schematically below:

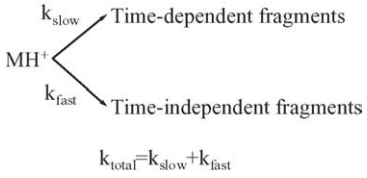

Microcanonical rate constants as a function of internal energy for the slow channel were calculated using RRKM. For the fast reaction pathway the rate–energy dependence is best described by a step function originating at the assumed threshold energy [23].

Fragmentation probability as a function of the internal energy of the parent ion and the experimental observation time (t_r), $F(E, t_r)$, is given by:

$$F(E, t_r) = e^{-(k_{total}(E)+k_{rad})t_r} \quad (1)$$

where k_{rad} is the rate constant for radiative cooling of the excited ion. Breakdown graph for dissociation of the parent ion into several fragments was constructed using formal kinetics equations corresponding to a specific reaction scheme.

The energy deposition function was described by the following analytical expression:

$$P(E, E_{coll}) = \frac{(E-\Delta)^l}{C} \exp\left(-\frac{E-\Delta}{f(E_{coll})}\right) \quad (2)$$

where l and Δ are parameters, $C = \Gamma(l+1)[f(E_{coll})]^{l+1}$ a normalization factor and $f(E_{coll})$ has the form:

$$f(E_{coll}) = A_2 E_{coll}^2 + A_1 E_{coll} + A_0 \quad (3)$$

where A_0, A_1 and A_2 are parameters, and E_{coll} is the collision energy. Finally, the normalized signal intensity for a particular reaction channel is given by the equation:

$$I_i(E_{coll}) = \int_0^\infty F_i(E, t_r) P(E, E_{coll})\, dE \quad (4)$$

Time- and collision energy-resolved SCs or fragmentation efficiency curves (TFECs) for different fragments were constructed using the above procedure and compared to experimental data. The energy deposition function was kept the same for all reaction times. Fitting parameters were varied until the best fit to experimental curves was obtained. These parameters included the critical energy and the activation entropy for the total decomposition of the precursor ion, the threshold for the fast fragmentation and parameters characterizing the energy deposition function (Eqs. (2) and (3)). The uniqueness of the fits was confirmed using sensitivity analysis described previously [16].

Vibrational frequencies of precursor ions were obtained from the frequency model given by Christie and co-workers [24]. Vibrational frequencies for the transition state were estimated by removing one C–N stretch (reaction coordinate) from the parent ion frequencies and varying all frequencies in the range of 500–1000 cm^{-1} to obtain the best fit with experimental data.

3. Results

In this study we examined fragmentation of singly protonated angiotensin III (RVYI**HP**F) and its four analogs: RVYI**HA**F, RVYI**HD**F, RVYI**FP**F and RVYI**YP**F. All peptides in this series contain arginine (R) as the most basic residue. Fragmentation of RVYIHAF and RVYIHDF has been briefly discussed in our previous study that focused on trends in the overall stability of peptide ions to dissociation rather than on mechanisms and detailed analysis of different dissociation pathways [19]. The second pair of peptides: RVYIFPF and RVYIYPF was selected to address the effect of histidine – the second most basic residue in the sequence – on the energetics and mechanisms of peptide fragmentation. It has been demonstrated that histidine protonation directs cleavage of a peptide bond at its C-terminal side [25]. For this series of peptides arginine is the preferred protonation site. However, because of the relatively high basicity of histidine (230 kcal/mol versus 248 kcal/mol for arginine) [26], some population of the parent ion could be protonated at the histidine residue rather than the arginine residue at high internal energies.

3.1. Fragmentation pathways

3.1.1. General trends

Fig. 1 shows a comparison of SID spectra of three peptides: RVYIHPF, RVYIFPF and RVYIYPF for 60 eV collisions with

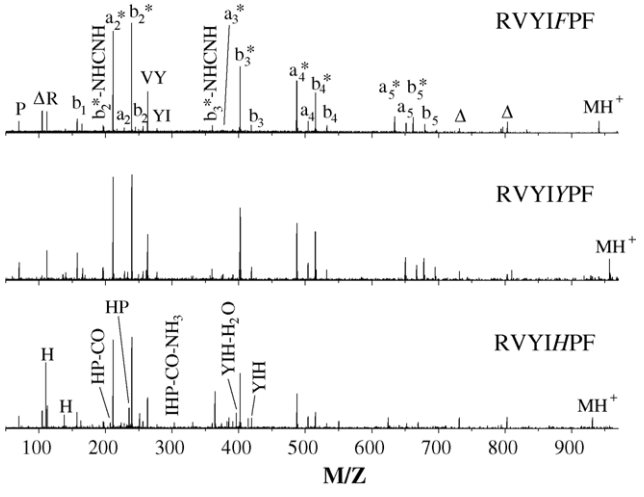

Fig. 1. 60 eV SID spectra of angiotensin III and its analogs obtained using FSAM surface as a target and reaction delay of 1 s. Δ denotes common noise peaks. Only unique fragment ions observed for RVYIHPF are labeled in the bottom spectrum. b_n-NH_3 and a_n-NH_3 ions are labeled as b_n^* and a_n^* in this figure.

Table 1
Relative abundance of major fragments of angiotensin III analogs normalized to the parent ion intensity obtained using 60 eV SID on the FSAM surface and 1 s reaction delay

Fragment ion	RVYI**HP**F	RVYI**HA**F	RVYI**HD**F	RVYI**YP**F	RVYI**FP**F
Backbone fragments					
b_1	1.2	0.6	1.1	1.1	1.0
b_2-NH_3-NHCNH	0.5			0.4	0.4
a_2-NH_3	5.9	5.7	5.9	4.2	4.1
a_2	0.4			0.4	0.3
b_2-NH_3	6.3	5.0	5.4	4.3	4.2
b_2	0.6	0.5	1.0	0.4	0.4
b_3-NH_3-NHCNH	0.5			0.5	0.3
a_3-NH_3	0.5	0.2		0.2	
b_3-$2NH_3$	0.8	0.3	0.3		
a_3	0.6			0.3	0.3
b_3-H_2O	0.6	0.3	0.3	0.5	0.4
b_3-NH_3	3.8	2.9	2.8	2.9	2.8
b_3	0.8	0.4	0.3	0.6	0.5
a_4-NH_3	2.4	1.5	1.5	2.3	2.3
a_4	1.0	0.5	1.2	0.8	0.7
b_4-NH_3	1.2	1.0	1.2	2.0	2.1
b_4	0.7	0.0	0.8	0.5	0.5
a_5-NH_3	0.9	0.2	0.4	1.0	1.0
a_5	0.0	0.0		0.7	0.8
b_5-NH_3	0.5	0.6	1.4	1.0	1.0
b_5	0.6	0.3	2.5	0.6	0.5
b_6-NH_3		0.3	0.9		
b_6			10.0		
$b_6 + H_2O$		0.2		0.5	0.4
Immonium ions and internal fragments					
P	0.9			0.7	0.6
H(1 1 0)	4.4	1.6	1.0		
R	1.6	0.8	0.5	1.2	1.2
H(1 3 8)	1.0	0.5	0.7		
YI	0.3			0.4	0.4
IH	1.1	0.8	1.1		
VY	2.2			1.9	2.0
YIH	0.8	0.3	0.3		
YIH-H_2O	1.1	0.6	0.4		
y_3b_6 ions	**HP**	**HA**	**HD**	**YP**	**FP**
	1.5	3.9	3.2	0.5	0.5

the FSAM surface and reaction delay of 1 s. Table 1 gives a summary of major peaks observed for all peptides in the series. Because the basic arginine residue is located at the N-terminus of these peptides, SID spectra are dominated by N-terminal fragments (e.g., b_n, a_n, b_n-NH_3, a_n-NH_3). Other major peaks include internal fragments and immonium ions. A small MH^+-NH_3 peak is present in low-energy (<50 eV collision energy) SID spectra. In addition, a small peak corresponding to the loss of the C-terminal amino acid ($b_6 + H_2O$) [27] was observed for all peptides. Interestingly, fragmentation patterns of RVYIFPF and RVYIYPF are almost identical. Fragmentation of both peptides results in formation of a series of very abundant b_n-NH_3 and a_n-NH_3 ions and less abundant b_n and a_n ions. A similar MS/MS spectrum of angiotensin III was obtained by Wysocki and co-workers using sustained off-resonance excitation (SORI-CID) in FT-ICR MS [25]. However, when arginine was replaced with a fixed-charge derivative (tris(2,4,6,-trimethoxyphenyl) phosphine) no peaks corresponding to loss of ammonia from backbone fragments were observed in the SORI-CID spectrum [25]. In addition to N-terminal backbone fragments just discussed SID, of angiotensin III analogs generates fragment ions corresponding to loss of 42 Da (NHCNH) from all abundant b_n-NH_3 and a_n-NH_3 ions, internal fragments—YI, VY and y_3b_6 ions formed by cleavage C-terminal to the sixth residue and N-terminal to the fourth residue (e.g., HP, FP, YP, HD or HA depending on the sequence), along with immonium ions P, R, Y.

Although the same backbone fragments are observed for histidine-containing peptides in the series they also produce a number of distinct fragment ions such as H (both at 110 and 138 Da), IH, YIH and YIH-H_2O. All these fragments are histidine-directed cleavages suggesting that some fraction of precursor ions is protonated at histidine at elevated internal energies. Comparison of all five peptides shows that the abundance of y_3b_6 ions for histidine-containing peptides (i.e., HP, HD, HA) is significantly higher than the relative abundance of FP and YP fragments of RVYIFPF and RVYIYPF, respectively. This finding is unexpected because histidine directs

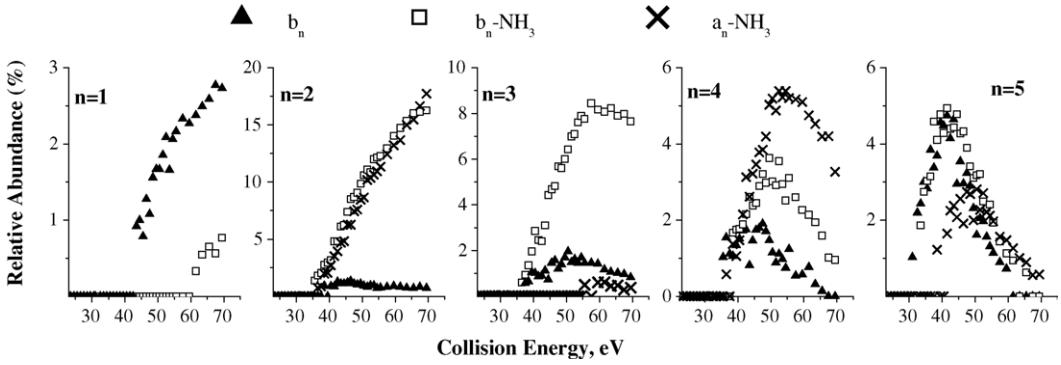

Fig. 2. Comparison of collision energy dependence of b_n, a_n and b_n-NH_3 ions of angiotensin III for $n = 1$–5 for 1 s reaction delay.

fragmentation C-terminal to itself; hence, this mechanism fails to account for the formation of abundant HP, HD and HA ions.

Singly protonated RVYIHDF contains both an arginine and an aspartic acid residues and undergoes selective fragmentation C-terminal to the aspartic acid [28–31]. This selective fragmentation is indicated by the large intensity of the b_6 ion. Consecutive fragmentation of this ion is responsible for increased abundance of the b_5 ion. Other fragments observed for this peptide are similar to fragment ions observed for the remaining peptides in the series.

3.1.2. Formation of b_n-NH_3 and a_n-NH_3 ions

Loss of ammonia from protonated arginine side chain facilitates formation of b_n-NH_3 or y_n-NH_3 fragments in MS/MS spectra of arginine-containing peptides. SID spectra shown in Fig. 1 indicate very facile formation of b_n-NH_3 and a_n-NH_3 fragments for angiotensin III analogs, some 2–10 times more abundant than the corresponding b_n and a_n ions. Several alternative pathways can account for facile formation of b_n-NH_3 and a_n-NH_3 ions. They can be formed by consecutive loss of ammonia from the corresponding b_n and a_n ions, consecutive backbone fragmentation of the MH^+-NH_3 ion or larger b_n-NH_3 ions, or directly from the precursor ion. It will be shown that time- and energy-resolved SID data distinguish between these pathways.

Fig. 2 shows a comparison of collision-energy dependent data for b_n, b_n-NH_3 and a_n-NH_3 ($n = 1$–5) fragments of angiotensin III for 1 s reaction delay. Interestingly, each family of curves shows a very different behavior suggesting that no single rule can account for the formation of b_n-NH_3 and a_n-NH_3 fragments. For example, for $n = 2$–5 all b_n and b_n-NH_3 fragments have the same experimental threshold. However, the branching ratio between these fragments varies dramatically as a function of size. Fragmentation efficiency curves (FECs) of b_5 and b_5-NH_3 perfectly overlap while the b_n/b_n-NH_3 ratio decreases from 1 to ca. 0.1 with decrease in n. It is unlikely that for $n = 2$–5 b_n-NH_3 ions are formed by consecutive dissociation of the corresponding b_n ions to any significant extent. However, the relative position of FECs of the b_1 and b_1-NH_3 fragments suggests that the latter ion could be produced from its corresponding b ion. Similar reasoning can be applied to describe the formation of a_n-NH_3 ions. For $n = 2$ and 4 both the experimental threshold and the abundance of these fragments are inconsistent with consecutive formation from the corresponding b_n, b_n-NH_3 or a_n ions (Fig. 3), while a_3-NH_3 and a_5-NH_3 are most likely formed by loss of CO from b_3-NH_3 and b_5-NH_3 fragments.

FECs of different b_n-NH_3 ions are compared in Fig. 4. The results indicate that smaller b_n-NH_3 ions ($n = 2$–4) can be formed from the b_5-NH_3 ion but the $4 \rightarrow 3 \rightarrow 2$ pathway for $n = 2$–4 ions is not supported. Further insight on the formation of b_n-NH_3 ions can be obtained by examining time-resolved fragmentation efficiency curves (TFECs). Consecutive pathways exhibit similar kinetic behavior. Fig. 5 shows TFECs for b_n-NH_3 ions ($n = 2$–5) at three delay times (5 ms, 50 ms and 1 s). While the b_5-NH_3 curves show significant time dependence TFECs of smaller fragments follow different kinetics—specifically, b_4-NH_3 ion does not show any time dependence, while b_3-NH_3 and b_2-NH_3 show very weak dependence on reaction delay time. These results

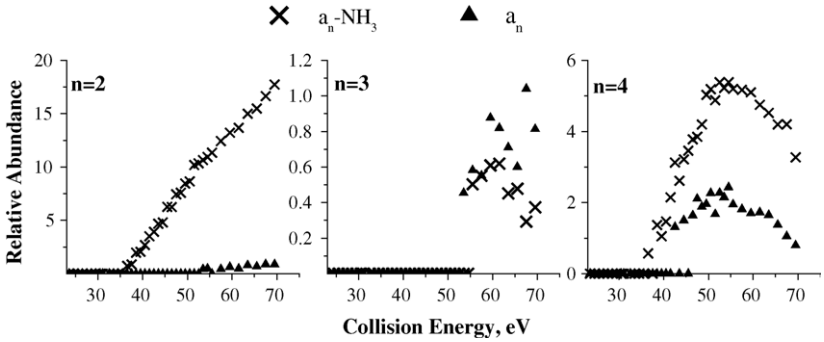

Fig. 3. Comparison of collision energy dependence of a_n and a_n-NH_3 ions of angiotensin III for $n = 2$–4 for 1 s reaction delay. For angiotensin III a_1 and a_5 ions were not observed in SID spectra.

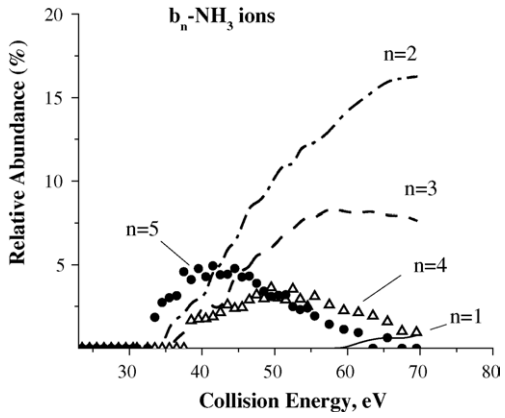

Fig. 4. Dependence of the relative abundance of b_n-NH_3 ions of angiotensin III on collision energy for 1 s reaction delay.

show that consecutive $5 \rightarrow 4$ fragmentation does not take place, while $5 \rightarrow 3$ and $5 \rightarrow 2$ reactions are not confirmed but cannot be ruled out based on qualitative comparison of their TFECs.

3.2. RRKM modeling

RRKM modeling of TFECs provides additional insight on the stability of peptides and their dissociation mechanisms. Relative stability is obtained from modeling of survival curves of different precursor ions, while more detailed modeling of individual reaction channels provides better understanding of mechanistic aspects of peptide fragmentation.

3.2.1. Effect of histidine on the relative stability of angiotensin III analogs

In our previous study we found that fragmentation of angiotensin analogs that do not contain an acidic residue is characterized by fairly high threshold energy (1.62 eV) and relatively high pre-exponential factor (ca. $10^{12}\,s^{-1}$). Survival curves for angiotensin III and its analogs (RVYIFPF and RVYIYPF) at two different delay times are shown in Fig. 6. The almost exact overlap between the curves suggests that the overall stability of these peptides towards dissociation is not affected by the presence of the histidine residue. Dissociation parameters shown in Table 2 obtained from the best fit of the experimental data are consistent with this suggestion. Both dissociation energies and activation entropies obtained for all three peptides are the same within the uncertainty of the model. It follows that, despite some differences in dissociation pathways described above, histidine presence does not affect the overall stability of angiotensin III analogs.

Table 2
Results of the RRKM modeling of the precursor ion survival curves

	RVYI**HP**F	RVYI**FP**F	RVYI**YP**F
DOF	396	405	408
E_0 (eV)	1.62	1.59	1.60
$\Delta S^{\ddagger}$ (e.u.)	−7.0	−6.9	−6.7
A (s^{-1})	7.6×10^{11}	7.9×10^{11}	8.6×10^{11}
E ($k = 1\,s^{-1}$) (eV)	7.8	7.6	7.7

E_0 is the threshold energy, $\Delta S^{\ddagger}$ the entropy change for the transition state, A the pre-exponential factor at 450 K, DOF the number of vibrational degrees of freedom and E ($k = 1\,s^{-1}$) is the internal energy corresponding to a rate constant of $1\,s^{-1}$.

3.2.2. Energetics of different dissociation pathways of angiotensin III

SID of angiotensin III analog results in formation of ca. 40 fragment ions. Because detailed modeling of such complex dissociation is not possible it is necessary to simplify the reaction scheme by combining fragments into several families. In this study we chose to model dissociation of the precursor ion of

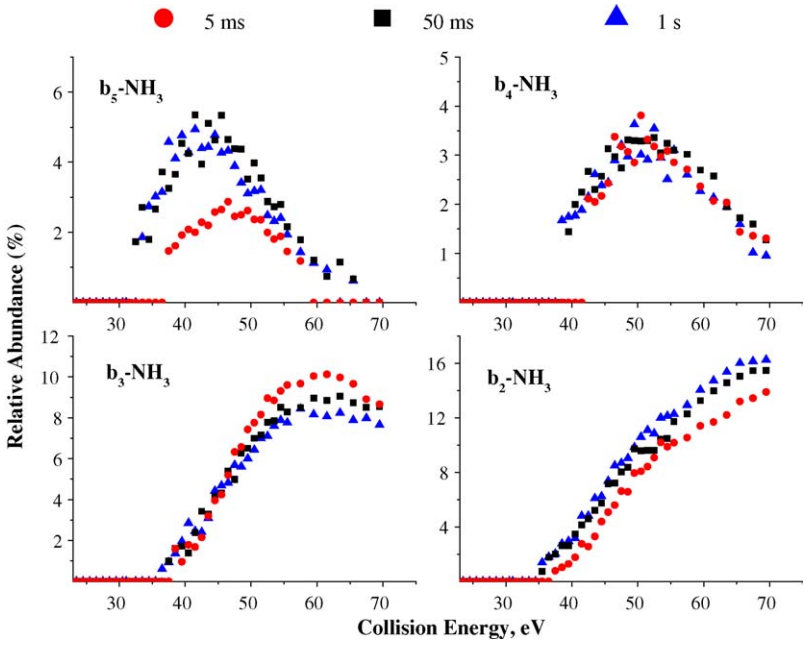

Fig. 5. Time- and energy-dependent fragmentation efficiency curves of b_n-NH_3 ions of angiotensin III.

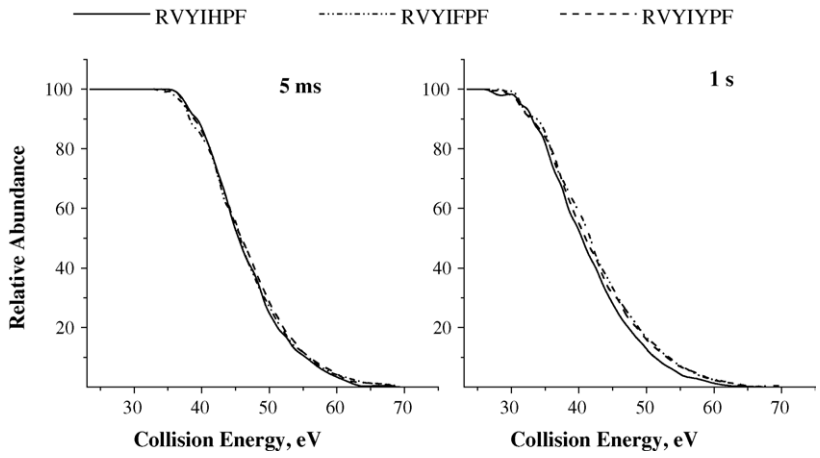

Fig. 6. Experimental survival curves for angiotensin III and its analogs at two reaction delays.

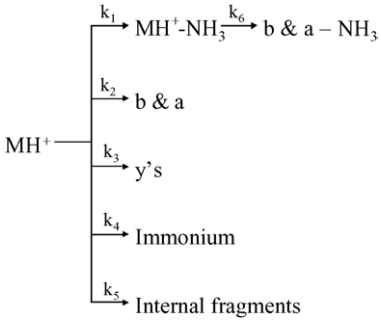

Scheme 1.

angiotensin III into six families of fragments: (1) MH^+-NH_3 ion, (2) b_n and a_n ions (b & a), (3) b_n-NH_3 and a_n-NH_3 ions (b & a-NH_3), (4) y_n ions, (5) internal fragments and (6) immonium ions. Although such modeling ignores the details of the TFECs of individual fragment ions it captures the major kinetics features.

Two dissociation schemes (Schemes 1 and 2) involving these families of fragments were evaluated in this study. Schemes 1 and 2 are the reactions used in RRKM modeling. The first scheme assumes that a_n-NH_3 and b_n-NH_3 ions are formed consecutively from the MH^+-NH_3 ion, while the second scheme assumes that all six families of fragment ions are formed directly from the precursor ion. In both schemes formation of each family of fragments is described using one rate constant calculated using RRKM/QET formalism. The breakdown graph is calculated using the appropriate equations of formal kinetics derived for each reaction scheme. The parameters of the energy deposition functions were obtained from modeling of total decomposition of the precursor ion as described earlier. Dissociation parameters characterizing the rate–energy dependence of six dissociation rate constants shown in Schemes 1 and 2 (critical energies and activation entropies) were varied to obtain the best fit of experimental TFECs at six different reaction delays.

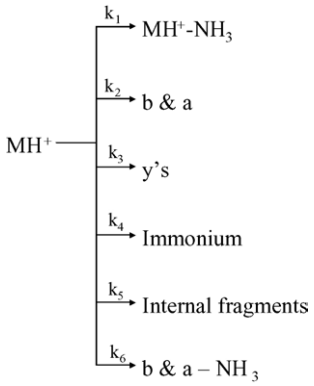

Scheme 2.

Fig. 7 shows the comparison between the experimental data corresponding to 1 s reaction delay and best fits obtained using Schemes 1 and 2. Because of simplifying assumptions of the modeling approach described above we do not expect a perfect overlap between the experimental data and the model. However, it is clear that Scheme 2 provides a poor fit for the MH^+-NH_3 ion and b and a ions, while Scheme 1 modeling achieves very good correspondence with experimental data. Dissociation parameters for reactions 1–5 obtained from the best fit are listed in Table 3. Microcanonical rate–energy dependences are shown in Fig. 8. The rate of reaction 6 was best described using a step function with threshold energy of 8.72 eV shown as a vertical line in the figure.

4. Discussion

4.1. Loss of ammonia from MH^+ and formation of b_n-NH_3 and a_n-NH_3 ions

Modeling of experimental TFECs suggests that most of b_n-NH_3 and a_n-NH_3 fragments of angiotensin III are formed by a very fast fragmentation of the MH^+-NH_3 ion. Reactions 1 and 6 in Scheme 1 account for ca. 55% of dissociation of the precursor ion. It is therefore not surprising that dissociation parameters obtained for reaction 1 (Table 3) closely resemble dissociation parameters obtained for modeling of the total decomposition of protonated angiotensin III (Table 2). Because fragmentation behavior of all peptides in the series except RVYIHDF is very similar it can be concluded that dissociation energies obtained

Table 3
Results of the RRKM modeling of the TFECs of different families of fragment ions of RVYIHPF

	MH^+-NH_3 k_1	b & a ions k_2	y ions k_3	Immonium ions k_4	Internal fragments k_5
E_0 (eV)	1.62	1.52	1.59	1.82	1.60
$\Delta S^{\ddagger}$ (e.u.)	−7.1	−14.5	−12.9	−3.4	−10.2
A (s^{-1})	7.1×10^{11}	1.7×10^{10}	3.9×10^{10}	4.7×10^{12}	1.5×10^{11}
E ($k = 1\ s^{-1}$) (eV)	7.8	8.2	8.6	9.0	8.1

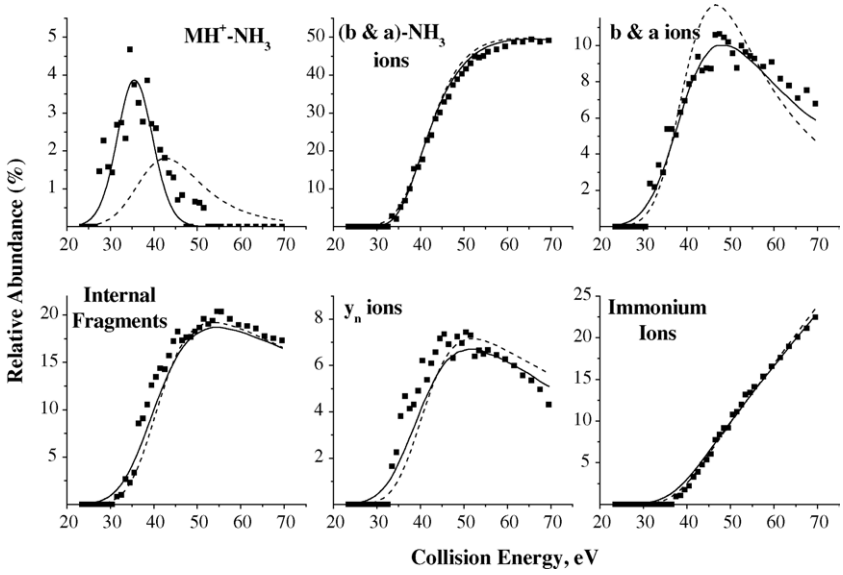

Fig. 7. RRKM modeling fit of experimental data for dissociation of RVYIHPF ($t = 1$ s) combined into major families of fragments (see text for details). Solid line corresponds to Scheme 1, dashed line corresponds to Scheme 2.

from modeling of survival curves of different precursor ions correspond to the barrier for loss of ammonia from the protonated arginine residue. The large values of ca. 1.6 eV obtained for all peptides that do not contain the aspartic acid residue are consistent with the mobile proton model that assumes that proton is sequestered by the basic arginine residue of a peptide [4].

Recently Csonka et al. reported a computational study on gas-phase fragmentation of protonated arginine [32]. They found that ammonia loss from arginine involves proton shift inside the guanidine group characterized by a very large energy barrier followed by heterolytic cleavage of the corresponding carbon–nitrogen bond. Scheme 3 shows a plausible pathway for NH_3 loss from angiotensin III that is in agreement with the computational study [32]. Loss of NH_3 results in formation of a protonated carbodiimide group. Formation of carbodiimide is supported by the

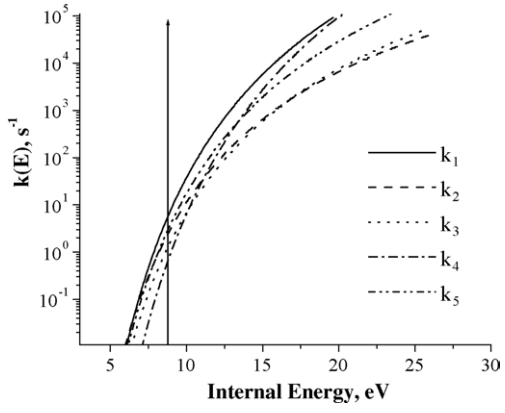

Fig. 8. Microcanonical rate–energy dependencies for the primary fragmentation pathways of singly protonated RVYIHPF; (—) reaction 1; (- - -) reaction 2; (···) reaction 3; (-·-·-) reaction 4; (-···-) reaction 5. Vertical line shows the onset of reaction 6.

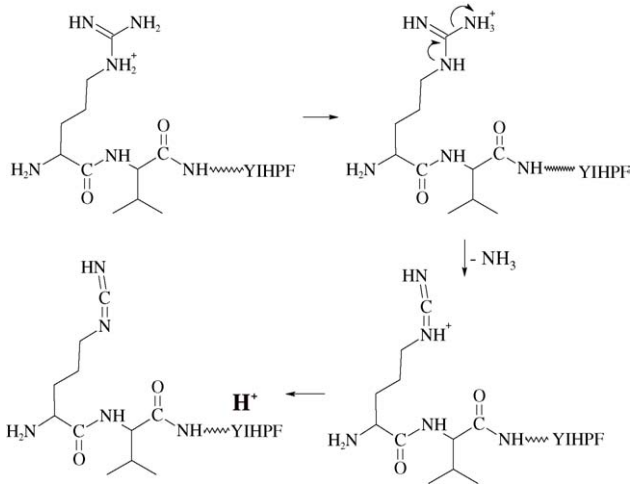

Scheme 3.

observation of NHCNH loss from a number of b_n-NH_3 ions (Table 1).

Proton affinity (PA) of carbodiimide (HNCNH) has been estimated by Cacace et al. [33] using experimentally determined PA of cyanamide (NH_2CN, 194.5 kcal/mol) and the difference in the heats of formation of these molecules. The reported PA of carbodiimide is 198.1 kcal/mol compared to 235.7 kcal/mol of the guanidine [34]. This study also demonstrated fast interconversion between carbodiimide and cyanamide. Such isomerization of the RNCNH side chain shown in Scheme 3 will result in formation of a more stable nitrile tautomer RNHCN. It follows that loss of ammonia from the arginine side chain converts the most basic residue in the peptide sequence into a residue with significantly lower PA that will subsequently transfer proton to a more favorable protonation site—to the imidazole ring of histidine or carbonyl oxygens along the peptide backbone. PA of histidine has been determined both experimentally (231.5 kcal/mol) [35] and theoretically (229.8 kcal/mol) [26], while PA of peptide backbone sites can be approximated using the data reported for polyglycines [36–38]. Because PAs of polyglycines increase with peptide size (e.g., from ca. 223.5 kcal/mol for Gly_2 to ca. 239.1 kcal/mol for Gly_6) we will use the midpoint value of 231 kcal/mol as a reasonable estimate of the PA of peptide backbone sites.

Thermochemical data suggest that proton transfer from the carbodiimide side chain to either the peptide backbone or to a more basic residue such as histidine is a favorable process with exothermicity of ca. 30 kcal/mol ("mobilized" proton is shown in bold in the last structure of Scheme 3). Because NH_3 loss is a slow process with fairly large KS of 6.2 eV for reaction time of 1 s, the excess internal energy of the MH^+-NH_3 ion following proton transfer to the backbone is larger than 7.5 eV. We conclude that loss of ammonia from angiotensin analogs results in formation of an ion with high internal excitation. In this highly internally excited ion the proton is not sequestered by any particular protonation site and is available to promote non-selective fragmentation resulting in facile formation of a variety of b_n-NH_3 and a_n-NH_3 ions. Our previous study on the energetics and dynamics of non-specific fragmentation of peptide ion of a similar complexity (LDIFSDF) [18] showed that the rate constant for subsequent fragmentation of the rearranged MH^+-NH_3 ion is at least five orders of magnitude higher than the rate constant for NH_3 loss. This explains the very fast dissociation of the MH^+-NH_3 ion demonstrated by our modeling of TFECs.

It is unlikely that the mechanism of NH_3 loss discussed in this section would be affected to a significant extent by the position of the arginine residue in peptide sequence. It follows that the same mechanism can play an important role in dissociation of tryptic peptides that contain basic arginine residues at the C-terminus. In the future we will address the influence of the position of basic residue in peptide sequence on NH_3 loss from protonated peptides.

4.2. Competing backbone fragmentation

Backbone fragmentation resulting in formation of a series of b_n and a_n ions in arginine-containing peptides requires proton transfer from protonated arginine to backbone carbonyl oxygens [2–6]. This step is similar to proton transfer within the guanidine group that precedes NH_3 loss and is expected to have a similar barrier. Consequently backbone fragmentation competes effectively with ammonia loss. Table 3 and Fig. 8 show that, even though b and a ion formation has a slightly lower barrier of 1.52 eV as compared to 1.62 eV required for ammonia loss, substantial rearrangements associated with formation of b and a ions significantly lowers activation entropy and slows these fragmentation channels. Tight transition states are found for all backbone cleavages resulting in formation of b and a ions, y ions and internal fragments. These entropic barriers may be attributed to peptide rearrangement resulting in solvation of the protonated arginine residue by carbonyl oxygens prior to proton transfer.

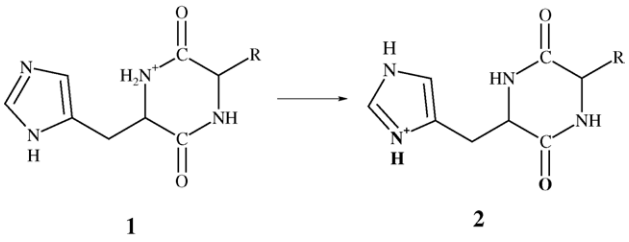

Scheme 4.

4.3. Formation of y_3b_6 ions

Formation of very abundant y_3b_6 ions in histidine-containing angiotensin III analogs (HP, HD and HA in Table 1) is a rather unexpected result because of the tendency of protonated histidine side chain to direct cleavage C-terminal to itself. Table 1 also shows that when histidine is replaced with tyrosine (Y) or phenylalanine (F) the relative abundance of y_3b_6 ions decreases by a factor of 3. These observations can be rationalized by assuming that y_3b_6 ions are not formed from histidine-protonated structures and that the relative abundance of these ions is determined by their thermochemical stability. O'Hair and co-workers found that histidine-containing b_2 ions have a diketopiperazine structure [39]. Ab initio calculations demonstrated that the most stable structure of the b_2 ion containing histidine and glycine (HG) is the histidine-protonated diketopiperazine (structure **2** in Scheme 4) [40]. Proton transfer from the diketopiperazine ring to the side chain shown in Scheme 4 results in ca. 20 kcal/mol stabilization of the b_2 ion. Isomerization of histidine-containing b_2 ions results in formation of very stable structures, rationalizing the observed high abundance of HX and XH ions in SID spectra. These ions are characteristic features for identification of histidine-containing peptides. O'Hair and co-workers showed that histidine-protonated HX ions are stabilized by hydrogen bonding between the nitrogen of the protonated side chain and the carbonyl oxygen of the diketopiperazine ring (highlighted bold in structure **2** of Scheme 4). Partial destabilization of this interaction in HP ion (**3**) because of the proline ring rationalizes the decreased formation of HP ion relative to HA and HD (Table 1).

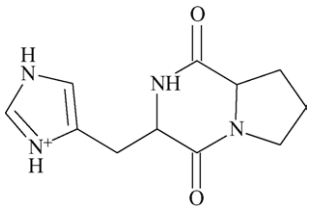

3

5. Conclusions

We have previously shown that time- and energy-resolved SID studies provide invaluable information on the energetics and dynamics of peptide fragmentation. In this work we demonstrated that detailed analysis of such data can provide a consistent mechanistic description of peptide fragmentation in tandem mass spectrometry. Comparison of TFECs of different backbone fragments of angiotensin III and its analogs suggested that b_n-NH_3 and a_n-NH_3 ions – major fragments of these peptides – are not produced consecutively from the corresponding b_n and a_n ions. Detailed modeling of TFECs of different families of fragment ions of angiotensin III demonstrated that these fragments are formed by very fast dissociation of the MH^+-NH_3 ion. Experimentally determined dissociation barrier for ammonia loss from the protonated arginine residue in a peptide is 1.6 eV. Loss of ammonia from the protonated arginine side chain releases the proton from the relatively unstable carbodiimide side chain and makes it available for non-specific backbone fragmentation. Stabilization of the MH^+-NH_3 ion via intramolecular proton transfer releases ca. 30 kcal/mol into vibrational excitation. This energy release combined with the initial excitation of the precursor ion rationalizes the very fast fragmentation of the MH^+-NH_3 ion found in our modeling. Comparison between the total decomposition rate of the precursor ion with the rate of NH_3 loss suggests that this pathway dominates gas-phase chemistry of the series of peptides examined in this study and determines their relative stability towards fragmentation.

Modeling of time-resolved survival curves of different peptides demonstrated that histidine does not alter their relative stability. In fact, dissociation parameters obtained for all peptides that do not contain an acidic aspartic acid residue are very similar—consistent with dominant role of the NH_3 loss from these peptides that is unaffected by the presence of histidine. However, peptide fragmentation patterns are strongly affected by histidine. In particular, internal fragments such as YIH and IH originating from dissociation of histidine-protonated ions become significant at high internal energy. HX and XH ions were also observed for histidine-containing peptides. High abundance of these fragments is rationalized by formation of highly stable structures of side chain-protonated diketopiperazine structures of histidine-containing b_2 ions as reported by O'Hair and co-workers [39,40]. Presence of these ions is a signature for histidine-containing peptides.

Acknowledgements

The research described in this manuscript was performed at the W.R. Wiley Environmental Molecular Sciences Laboratory (EMSL), a national scientific user facility sponsored by the U.S. Department of Energy's Office of Biological and Environmental Research and located at Pacific Northwest National Laboratory (PNNL). PNNL is operated by Battelle for the U.S. Department of Energy. Research at EMSL was supported by the grant from the Chemical Sciences Division, Office of Basic Energy Sciences of the U.S. Department of Energy. Financial support for T.H.B. was provided through NSF grant CHE-9634238. We thank Prof. Richard O'Hair for very helpful discussions.

References

[1] R. Aebersold, D.R. Goodlett, Chem. Rev. 101 (2001) 269.
[2] R.A.J. O'Hair, J. Mass Spectrom. 35 (2000) 1377.
[3] M.J. Polce, D. Ren, C. Wesdemiotis, J. Mass Spectrom. 35 (2000) 1391.
[4] V.H. Wysocki, G. Tsaprailis, L.L. Smith, L.A. Breci, J. Mass Spectrom. 35 (2000) 1399.
[5] A. Schlosser, W.D. Lehmann, J. Mass Spectrom. 35 (2000) 1382.
[6] B. Paizs, S. Suhai, Mass Spectrom. Rev. 24 (2005) 508.
[7] C. Lifshitz, Eur. J. Mass Spectrom. 8 (2002) 85.
[8] S.A. McLuckey, D.E. Goeringer, J. Mass Spectrom. 32 (1997) 461.
[9] J. Laskin, E. Denisov, J. Futrell, J. Phys. Chem. B 105 (2001) 1895.
[10] M.D.A. Mabud, M.J. Dekrey, R.G. Cooks, Int. J. Mass Spectrom. Ion Process. 67 (1985) 285.
[11] R.G. Cooks, T. Ast, T. Pradeep, V. Wysocki, Acc. Chem. Res. 27 (1994) 316.
[12] O. Meroueh, W.L. Hase, J. Am. Chem. Soc. 124 (2002) 1524.
[13] J. Laskin, J.H. Futrell, Mass Spectrom. Rev. 22 (2003) 158.
[14] J. Laskin, J.H. Futrell, J. Am. Soc. Mass Spectrom. 14 (2003) 1340.
[15] J. Laskin, M. Byrd, J. Futrell, Int. J. Mass Spectrom. 196 (2000) 285.
[16] J. Laskin, J. Futrell, J. Phys. Chem. A 104 (2000) 5484.
[17] J. Laskin, E. Denisov, J.H. Futrell, Int. J. Mass Spectrom. 219 (2002) 189.
[18] T.H. Bailey, J. Laskin, J.H. Futrell, Int. J. Mass Spectrom. 222 (2003) 313.
[19] J. Laskin, T.H. Bailey, J.H. Futrell, Int. J. Mass Spectrom. 234 (2004) 89.
[20] J. Laskin, E.V. Denisov, A.K. Shukla, S.E. Barlow, J.H. Futrell, Anal. Chem. 74 (2002) 3255.
[21] S.A. Shaffer, K.Q. Tang, G.A. Anderson, D.C. Prior, H.R. Udseth, R.D. Smith, Rapid Commun. Mass Spectrom. 11 (1997) 1813.
[22] M.W. Senko, J.D. Canterbury, S.H. Guan, A.G. Marshall, Rapid Commun. Mass Spectrom. 10 (1996) 1839.
[23] J. Laskin, T.H. Bailey, J.H. Futrell, J. Am. Chem. Soc. 125 (2003) 1625.
[24] P.J. Derrick, P.M. Loyd, J.R. Christie, in: I. Cornides, G. Howárth, K. Vékey (Eds.), Advances in Mass Spectrometry, vol. 13, Wiley, Chichester, 1995.
[25] G. Tsaprailis, H. Nair, W. Zhong, K. Kuppannan, J.H. Futrell, V.H. Wysocki, Anal. Chem. 76 (2004) 2083.
[26] Z.B. Maksic, B. Kovacevic, Chem. Phys. Lett. 307 (1999) 497.
[27] G.C. Thorne, K.D. Ballard, S.J. Gaskell, J. Am. Soc. Mass Spectrom. 1 (1990) 249.
[28] W. Yu, J.E. Vath, M.C. Huberty, S.A. Martin, Anal. Chem. 65 (1993) 3015.
[29] J. Qin, B.T. Chait, J. Am. Chem. Soc. 117 (1995) 5411.
[30] S.G. Summerfield, A. Whiting, S.J. Gaskell, Int. J. Mass Spectrom. Ion Process. 162 (1997) 149.
[31] G. Tsaprailis, H. Nair, A. Somogyi, V.H. Wysocki, W.Q. Zhong, J.H. Futrell, S.G. Summerfield, S.J. Gaskell, J. Am. Chem. Soc. 121 (1999) 5142.
[32] I.P. Csonka, B. Paizs, S. Suhai, J. Mass Spectrom. 39 (2004) 1025.

[33] F. Cacace, G. Depetris, F. Grandinetti, G. Occhiucci, J. Phys. Chem. 97 (1993) 4239.
[34] Data from NIST Standard Reference Database 69, June 2005 Release: NIST Chemistry WebBook.
[35] A.G. Harrison, Mass Spectrom. Rev. 16 (1997) 201.
[36] Z.C. Wu, C. Fenselau, J. Am. Soc. Mass Spectrom. 3 (1992) 863.
[37] J.Y. Wu, C.B. Lebrilla, J. Am. Chem. Soc. 115 (1993) 3270.
[38] K. Zhang, D.M. Zimmerman, A. Chungphillips, C.J. Cassady, J. Am. Chem. Soc. 115 (1993) 10812.
[39] J.M. Farrugia, R.A.J. O'Hair, G.E. Reid, Int. J. Mass Spectrom. 210 (2001) 71.
[40] J.M. Farrugia, T. Taverner, R.A.J. O'Hair, Int. J. Mass Spectrom. 209 (2001) 99.